JACS
JOURNAL OF THE AMERICAN CHEMICAL SOCIETY
Article
pubs.acs.org/JACS

Hypercoordinate Ketone Adducts of Electrophilic η^3-H_2SiRR' Ligands on Ruthenium as Key Intermediates for Efficient and Robust Catalytic Hydrosilation

Mark C. Lipke and T. Don Tilley*

Department of Chemistry, University of California, Berkeley, Berkeley, California 94720-1460, United States

Supporting Information

ABSTRACT: The electrophilic η^3-H_2SiRR' σ-complexes $[PhBP^{Ph}_3]RuH(\eta^3\text{-}H_2SiRR')$ (RR′ = MePh, **1a**; Ph_2, **1b**; $[PhBP^{Ph}_3]^-$ = $[PhB(CH_2PPh_2)_3]^-$) are efficient catalysts (0.01−2.5 mol % loading) for the hydrosilation of ketones with $PhMeSiH_2$, Ph_2SiH_2, or $EtMe_2SiH$. An alkoxy complex $[PhBP^{Ph}_3]Ru{-}OCHPh_2$ (**4b**) was observed (by $^{31}P\{^1H\}$ NMR spectroscopy) as the catalyst resting state during hydrosilation of benzophenone with $EtMe_2SiH$. A different catalyst resting state was observed for reactions using $PhMeSiH_2$ or Ph_2SiH_2, and was identified as a silane σ-complex $[PhBP^{Ph}_3]RuH[\eta^2\text{-}H{-}SiRR'(OCHPh_2)]$ (RR′ = MePh, **5a**; Ph_2, **5b**) using variable temperature multinuclear NMR spectroscopy (−80 to 20 °C). The hydrosilation of benzophenone with $PhMeSiH_2$ and **1a** was examined by ^1H NMR spectroscopy at −18 °C (in CD_2Cl_2), and this revealed that either **1a**, **5a**, or both **1a** and **5a** could be observed as resting states of the catalytic cycle, depending on the initial $[PhMeSiH_2]$:[benzophenone] ratio. Kinetic studies revealed two possible expressions for the rate of product formation, depending on which catalyst resting state was present (rate = $k_{obs}[PhMeSiH_2][\mathbf{5a}]$ and rate = k'_{obs}[benzophenone][**1a**]). Computational methods (DFT, b3pw91, 6-31G(d,p)/LANL2DZ) were used to determine a model catalytic cycle for the hydrosilation of acetone with $PhMeSiH_2$. A key step in this mechanism involves coordination of acetone to the silicon center of **1a-DFT**, which leads to insertion of the carbonyl group into an Si−H bond (that is part of a Ru−H—Si 3c−2e bond). This generates an intermediate analogous to **5a** (**5a-i-DFT**), and the final product is displaced from **5a-i-DFT** by an associative process involving $PhMeSiH_2$.

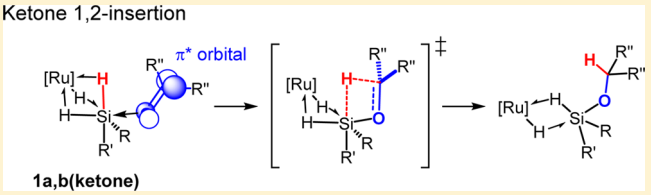

INTRODUCTION

Transition metal catalyzed carbonyl hydrosilation reactions are useful for the reduction of ketones, aldehydes, and esters under mild conditions.[1] There is considerable interest in understanding the mechanisms of these transformations, and a variety of catalytic cycles have been proposed.[2−5] Recently developed mechanistic proposals feature the attack of a ketone substrate at an electrophilic silicon center in the coordination sphere of the transition metal catalyst (Scheme 1). For example, it has been proposed that cationic rhodium complexes might activate secondary silanes to generate a silylene dihydride complex as a key intermediate responsible for binding the ketone substrate (path A).[4] Investigation of this mechanistic hypothesis has been somewhat hampered by the fact that silylene complexes have not been isolated or otherwise clearly detected for the relevant, rhodium-based catalysts.[1d,4] Isolated silylene complexes of other transition metals exhibit high reactivities toward carbonyl compounds, and this includes examples of catalytic ketone hydrosilation reactions.[6] However, detailed mechanistic investigations are lacking for these catalytic systems, and thus the silylene complexes have not been confirmed as participants in the catalytic cycles for these reactions.

Cationic iridium and ruthenium $R_3Si{-}H$ σ-complexes have also been suggested to participate as key electrophilic intermediates in catalytic ketone hydrosilation reactions (path B).[5] For these mechanistic proposals, attack of the ketone substrate at silicon results in heterolytic cleavage of the coordinated Si−H bond. This transfers a silyl cation to the ketone substrate to produce an $[R_3Si{-}O{=}CR_2]^+$ species, which can then accept a hydride from the metal. Experimental and computational investigations have presented support for this type of mechanism,[5] and related pathways might be important in hydrosilations of other substrates (e.g., nitriles, amides, pyridines), which exhibit high selectivities for specific products (e.g., N-silylimines,[7a,b] *N*-silyl amines,[7c] *N*-silyl-1,4-dihydropyridines,[7d] respectively). Considering the apparent variety of possible carbonyl hydrosilation mechanisms involving electrophilic silicon species, and the general lack of detailed mechanistic understanding, it is important to define specific pathways of this type in more detail. A deeper understanding of these mechanisms could provide insight into the selectivities of hydrosilation reactions (e.g., enantioselectivity or 1,2- vs 1,4-regioselectivity for α,β-unsaturated ketones),[3,4] as well as aid in the development of new hydrosilation reactions and improved catalysts.

With these factors in mind, we examined electrophilic η^3-H_2SiRR' σ-complexes of the type $[PhBP^{Ph}_3]RuH(\eta^3\text{-}H_2SiRR')$

Received: September 3, 2014

   dx.doi.org/10.1021/ja509073c | J. Am. Chem. Soc. XXXX, XXX, XXX−XXX

Scheme 1. Involvement of Electrophilic Silicon in Transition Metal Catalyzed Hydrosilation Reactions

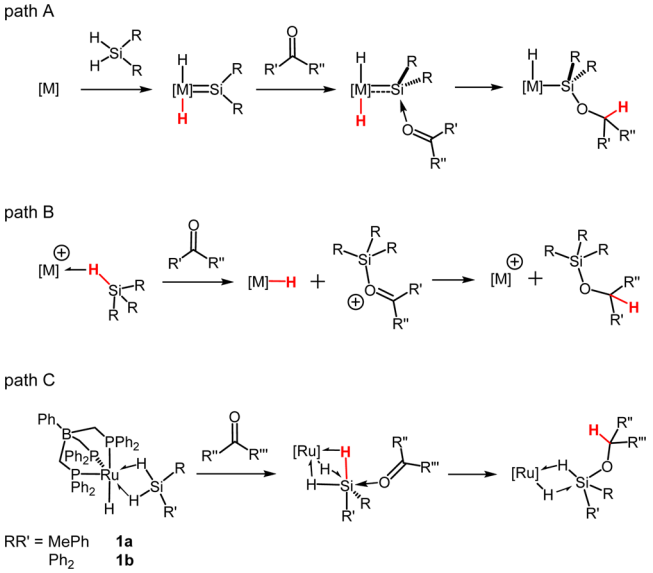

(RR′ = PhMe, **1a**; Ph_2, **1b**; Scheme 1, path C) as possible catalysts for ketone hydrosilation. This was particularly interesting in light of the discovery that **1a,b** react with Lewis bases to form unusual adducts of the type $[PhBP^{Ph}_3]Ru(\mu\text{-}H)_3SiRR'(base)$,[8] and that adducts of this type are important intermediates for a stoichiometric hydrosilation reaction involving XylNC (Xyl = 2,6-$Me_2C_6H_3$) and **1a,b**.[9] Indeed, as shown here, complexes **1a,b** are efficient catalysts for the hydrosilation of electron-rich and electron-poor ketones. These are the first examples of catalytic transformations involving η^3-H_2SiRR' σ-complexes, and a detailed mechanistic investigation was undertaken to examine the role of the η^3-H_2SiRR' ligands in this catalysis. These studies reveal that the binding of a ketone to the silicon center of **1a,b** activates the ketone toward insertion into a partially activated (coordinated) Si−H bond. Notably, this mechanism exhibits key features of both the silylene mechanism (i.e., involvement of an electrophilic silicon center derived from the activation of two Si−H bonds)[4] and the σ-silane mechanism (i.e., electrophilic Si−H σ-complexes as key intermediates).[5] Additionally, the involvement of a six-coordinate silicon intermediate (e.g., $[PhBP^{Ph}_3]Ru(\mu\text{-}H)_3Si(RR')\leftarrow O{=}CR''R'''$) is a unique feature of the η^3-H_2SiRR' mechanism for the hydrosilation of ketones.

RESULTS AND DISCUSSION

Hydrosilation of Ketones Catalyzed by 1a. The catalytic hydrosilation of benzophenones with a variety of silanes was examined for initial screening of the catalytic activity of the η^3-H_2SiRR' complex **1a** (eq 1, Table 1). Addition of

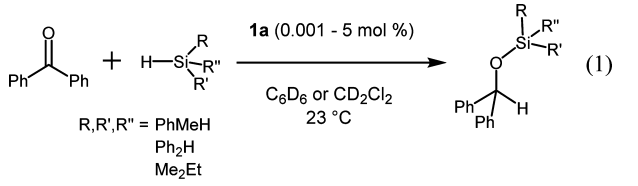

(1)

benzophenone (in benzene-d_6) to a pale yellow solution of $PhMeSiH_2$ (1.1 equiv) and 1 mol % **1a** (in benzene-d_6) resulted in an immediate change in color to golden yellow. After 15 min,

Table 1. Hydosilation of Benzophenone Catalyzed by 1a[a]

Entry	Silane	**1a** (mol %)	Time (h)	Yield (%)[b]
1	$PhMeSiH_2$	1	0.25	100
2	$PhMeSiH_2$	1[c]	0.25	100
3[d]	$PhMeSiH_2$	0.01	3	81
			24	100
4[d]	$PhMeSiH_2$	0.001	48	46
5	Ph_2SiH_2	1	24	66
6	Ph_2SiH_2	5	24	97
7	$^iPr_2SiH_2$	2.5	24	0
8[e]	$^iPr_2SiH_2$	2.5	24	0
9	$EtMe_2SiH$	5	24	0
10[f]	$EtMe_2SiH$	1	1.5	100
11[f,g]	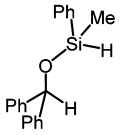	1	5	100

[a]At 23 °C in C_6D_6. [b]Determined by ^1H NMR using a C_6Me_6 internal standard. [c]Generated *in situ* from $PhMeSiH_2$ and **2**. [d]Neat $PhMeSiH_2$ as solvent. [e]At 60 °C in C_6D_6. [f]At 23 °C in CD_2Cl_2. [g]PhMe(Ph$_2$HCO)SiH substrate generated *in situ* as an intermediate in the reaction of $PhMeSiH_2$ with 2 equiv of benzophenone.

the yellow color had faded substantially (back to pale yellow) and the ^1H NMR spectrum of the mixture revealed quantitative formation of the expected 1,2-hydrosilation product PhMeH-Si−O—$CHPh_2$ (Table 1, entry 1). Identical results were obtained when **1a** was generated *in situ* from $PhMeSiH_2$ and $\{[PhBP^{Ph}_3]Ru(\mu\text{-}Cl)\}_2$ (**2**) prior to addition of benzophenone (Table 1, entry 2). Very low catalyst loadings were effective for the hydrosilation of benzophenone with $PhMeSiH_2$. With 0.01 mol % of **1a** in neat $PhMeSiH_2$, 81% conversion of benzophenone was observed after 3 h, and quantitative yield was achieved after 24 h (Table 1, entry 3). At an even lower catalyst loading (0.001 mol % **1a**), a 46% yield was achieved after 48 h (Table 1, entry 4). These results (TOF = 45 s^{-1} and TON = 4.6×10^4) demonstrate that **1a** is a highly efficient catalyst for the hydrosilation of benzophenone.[10]

The catalytic hydrosilation of benzophenone was less efficient with Ph_2SiH_2 (Table 1, entries 5 and 6), and did not proceed at all with $^iPr_2SiH_2$ (entries 7 and 8). For the latter reaction, the addition of $^iPr_2SiH_2$ to **1a** initially resulted in the displacement of $PhMeSiH_2$ (by ^1H NMR spectroscopy) and the observation of a new Ru−H resonance that is consistent with the formation of $[PhBP^{Ph}_3]RuH(\eta^3\text{-}H_2Si^iPr_2)$ (^1H δ −7.45 ppm) as the major $[PhBP^{Ph}_3]Ru$ species (>90%) in solution.[8] After heating to 60 °C, this species had entirely converted into the η^5-cyclohexadienyl complex $[PhBP^{Ph}_3]Ru(\eta^5\text{-}C_6D_6H)$ (**3-d_6**, observed by ^1H and $^{31}P\{^1H\}$ NMR spectroscopy).[11] Thus, it appears that for this example, catalyst deactivation by formation of **3-d_6** is faster than reaction of the η^3-$H_2Si^iPr_2$ complex with benzophenone.

The hydrosilation of benzophenone was also ineffective under these conditions when using a relatively small tertiary silane substrate ($EtMe_2SiH$, Table 1, entry 9). In this case, the formation of **3-d_6** was evident (by ^1H and $^{31}P\{^1H\}$ NMR spectroscopy) after addition of **1a** to the reactants in benzene-

dx.doi.org/10.1021/ja509073c | J. Am. Chem. Soc. XXXX, XXX, XXX−XXX

d_6. The rapid formation of **3-d_6** may be due to the lower stability of [PhBP$^{Ph}_3$]RuH(η^2-H−SiMe$_2$Et) complexes, relative to the η^3-H$_2$SiRR′ complexes involving secondary silanes. However, the hydrosilation reaction with EtMe$_2$SiH proceeds in CD_2Cl_2 to give the hydrosilation product in quantitative yield (Table 1, entry 10). Similarly, 2 equiv of benzophenone undergo quantitative hydrosilation with PhMeSiH$_2$ to form PhMeSi(OCHPh$_2$)$_2$ when using CD_2Cl_2 as the solvent (Table 1, entry 11), whereas the reaction stops at the formation of PhMeHSi−OCHPh$_2$ when C_6D_6 is the solvent. Notably, for hydrosilation using EtMe$_2$SiH, the reaction solution was orange in color rather than the golden yellow color consistently observed for reactions utilizing Ph$_2$SiH$_2$ or PhMeSiH$_2$. This observation suggested that different resting states might be present for hydrosilation using tertiary silanes or secondary silanes, and this possibility was confirmed by NMR spectroscopy. The ^{1}H and ^{31}P{^{1}H} NMR spectra of the reaction solutions indicate that the resting state for the catalytic cycle is an alkoxide complex [PhBP$^{Ph}_3$]Ru−O—CHPh$_2$ (**4b**) when EtMe$_2$SiH is the silane substrate, and an Si−H σ-complex of the type [PhBP$^{Ph}_3$]Ru(H)[η^2-H−SiRR′(OCHPh$_2$)] (RR′ = MePh, **5a**; RR′ = Ph$_2$, **5b**) for the secondary silane substrates (see mechanistic investigation below for complete discussion of isolation and characterization of **4b**, and *in situ* observation and characterization of **5a**,**b**).

Several additional ketones were examined as substrates for catalytic hydrosilation with PhMeSiH$_2$, using **1a** as the catalyst (eq 2, Table 2). A variety of 4-substituted and 4,4′-disubstituted

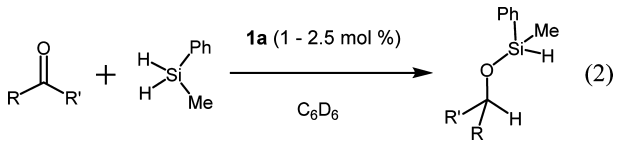

benzophenones underwent quantitative hydrosilation within 20 min at room temperature (1.1 equiv of PhMeSiH$_2$ and 1 mol % **1a** in benzene-d_6). The substituted benzophenones ranged from electron rich (4-methyoxy, Table 2, entry 5) to electron poor (4,4′-difluoro, entry 6), and thus the electronic properties of the benzophenone substrates do not appear to substantially affect the rate or yield of catalytic hydrosilation.

Table 2. Hydosilation of Ketones Using PhMeSiH$_2$ Catalyzed by 1a[a]

entry	ketone (RR′C═O)	**1a** (mol %)	time (h)	yield (%)[b]
1	*p*-C$_6$H$_4$F, Ph	1	0.3	100
2	*p*-C$_6$H$_4$Cl, Ph	1	0.3	100
3	*p*-C$_6$H$_4$Br, Ph	1	0.3	100
4	*p*-C$_6$H$_4$Me, Ph	1	0.3	100
5	*p*-C$_6$H$_4$OMe, Ph	1	0.3	100
6	*p*-C$_6$H$_4$F, *p*-C$_6$H$_4$F	1	0.3	100
7	*p*-C$_6$H$_4$Cl, *p*-C$_6$H$_4$Cl	1	0.3	100
8	*p*-C$_6$H$_4$Br, *p*-C$_6$H$_4$Br	1	0.3	100
9	*p*-C$_6$H$_4$Me, *p*-C$_6$H$_4$Me	1	0.3	100
10	Ph, Me	1	0.5	44
11	Ph, Me	2.5	0.25	90
12	Ph, cyclopropyl	1	0.5	100
13	cyclopentanone	1	0.75	65[c]/35[d]
14	C$_6$F$_5$, Me	1	24	69
15	C$_6$F$_5$, Me	2.5	24	90
16[e]	Ph, CF$_3$	2.5	24	75

[a]Room temperature in C_6D_6. [b]Determined by ^{1}H NMR using a C_6Me_6 internal standard. [c]Cyclopentyl silyl ether product [d]Cyclopentenyl silyl ether product [e]Heated to 80 °C in C_6D_6.

Acetophenone was also effective as a substrate, but required a higher catalyst loading to achieve full conversion (Table 2, entries 10 and 11), due to deactivation of the catalyst by formation of **3-d_6**. At full conversion of acetopheonone, a 90% yield of the hydrosilation product was observed by ^{1}H NMR spectroscopy, along with at least one minor organic side product that was not identified. Cyclopentanone was also converted to more than one product (Table 2, entry 13), and in this case the selectivity for the hydrosilation product was even lower (65% yield at full conversion of cyclopentanone). The 1-cyclopentenyl silyl ether C$_5$H$_7$—O−SiHMePh was identified as the other product formed (35% yield), and thus activation of the α-C−H bonds of the ketone competes with hydrosilation in this case. However, this was not observed for cyclopropyl phenyl ketone, which underwent hydrosilation with similar efficiency to that of the benzophenones (Table 2, entry 12).

Fluorinated acetophenones were also effective substrates, but the reactions proceeded slower than with benzophenones or acetophenone. With 1,2,3,4,5-pentafluoroacetophenone, the reaction required a much longer time (24 h) and higher catalyst loading (2.5 mol %) to achieve a high yield of the hydrosilation product (Table 2, entries 14 and 15). Catalytic hydrosilation of α,α,α-trifluoroacetophenone was even less efficient, and required heating to 80 °C for hydrosilation at an appreciable rate (Table 2, entry 16). The lower reactivity with these electron-deficient substrates is consistent with the possible role of the electrophilic η^3-H$_2$SiRR′ ligand in catalysis, since binding of these substrates to silicon would be less favorable than for more nucleophilic ketones.

Mechanistic Investigations with Stoichiometric Reactions. The carbonyl hydrosilation reactions described above are the first examples of catalytic activity involving η^3-H$_2$SiRR′ complexes (**1a**,**b**).[8] Thus, it was of interest to examine what role the η^3-H$_2$SiRR′ ligand might have in the mechanism of these catalytic hydrosilations. We previously observed the ability of XylNC to undergo 1,1-insertion into an Si−H bond of the adducts [PhBP$^{Ph}_3$]Ru(μ-H)$_3$Si(RR′)←CNXyl (RR′ = MePh, **1a(CNXyl)**; RR′ = Ph$_2$, **1b(CNXyl)**),[9] and it seems possible that a similar reaction step might play a key role in the 1,2-hydrosilation of ketones (Scheme 2). However, in **1a**,**b-(CNXyl)**, the C≡N π^* orbital is well positioned to accept a hydride, and this may not be true for the C═O π^* orbital in

Scheme 2. 1,1- and 1,2-Insertions into the Si−H Bond of [PhBP$^{Ph}_3$]Ru(μ-H)$_3$Si(RR′)←(Substrate)

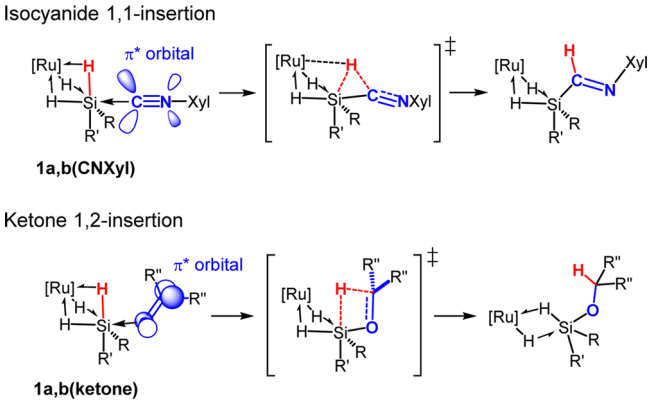

dx.doi.org/10.1021/ja509073c | J. Am. Chem. Soc. XXXX, XXX, XXX−XXX

the ketone adducts $[PhBP^{Ph}_3]Ru(\mu\text{-}H)_3Si(RR')\leftarrow O{=}CR''R'''$ ($O{=}CR''R'''$ = ketone substrate; RR′ = MePh, **1a(ketone)**; RR′ = Ph_2, **1b(ketone)**). In these latter species, the ketone is expected to bind via an sp^2 hybridized lone pair on oxygen, and this positions the C=O π^* orbital such that it is orthogonal to the nearest hydride ligand (Scheme 2). Thus, the ketone must rotate away from its ideal bonding geometry in order for the carbonyl group to insert into the Si−H bond of **1a**,**b(ketone)**, and this requirement could prevent such a mechanism from being active for the hydrosilation of ketones. Additionally, a mechanism that does not involve an η^3-H_2SiRR' complex must be possible, as is evident from the hydrosilation reactions using $EtMe_2SiH$. Thus, additional information on possible hydrosilation mechanisms was sought, and the hydrosilation of benzophenone was chosen for detailed examination since this substrate cleanly provides the hydrosilation product in high yields using $PhMeSiH_2$, Ph_2SiH_2, or $EtMe_2SiH$.

During the hydrosilation with $EtMe_2SiH$, it was possible to observe a new $^{31}P\{^1H\}$ NMR resonance (δ 78.45 ppm in CD_2Cl_2) near that previously reported for the *tert*-butoxy complex $[PhBP^{Ph}_3]RuO^tBu$ ($^{31}P\{^1H\}$ δ 80.44 ppm in CD_2Cl_2, **4a**).[9] This latter species reacts with $EtMe_2SiH$ in benzene-d_6 to quantitatively form $EtMe_2Si{-}O{-}{}^tBu$ and **3-d_6**.[11] Thus, it seemed possible that the observed intermediate species might be a related diphenylmethoxy complex $[PhBP^{Ph}_3]Ru{-}OCHPh_2$ (**4b**), and that reaction of this species with $EtMe_2SiH$ forms the hydrosilation product $EtMe_2Si{-}O{-}CHPh_2$ (Scheme 3). This

Scheme 3. Possible Catalytic Cycle for Hydrosilation of Benzophenone Using $EtMe_2SiH$

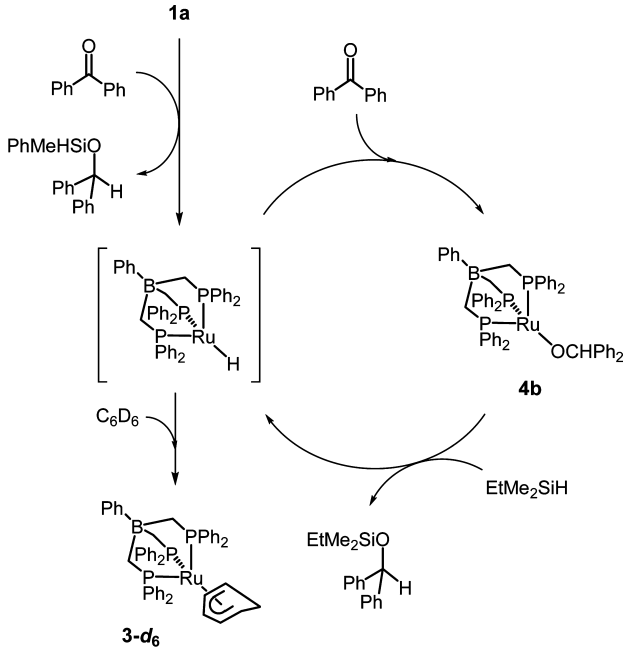

should also generate $[PhBP^{Ph}_3]Ru{-}H$, or a reactive adduct of this hydride species with a weakly coordinating ligand (e.g., $[PhBP^{Ph}_3]Ru(H)(L)$, L = solvent, product, $EtMe_2SiH$). Insertion of benzophenone into the Ru−H bond would regenerate **4b**, thus allowing for catalytic turnover. Benzene can compete with benzophenone for insertion into the Ru−H bond, and rapid formation of the catalytically inactive species **3-d_6** would explain the lack of catalysis when using C_6D_6 as the solvent and $EtMe_2SiH$ as the silane.

Complex **4b** was isolated in analytically pure form following an independent synthesis involving treatment of $\{[PhBP^{Ph}_3]Ru(\mu\text{-}Cl)\}_2$ (**2**) with 2 equiv of the diphenylmethoxide salt $NaOCHPh_2$ (eq 3). The $^{31}P\{^1H\}$ NMR spectrum of **4b**

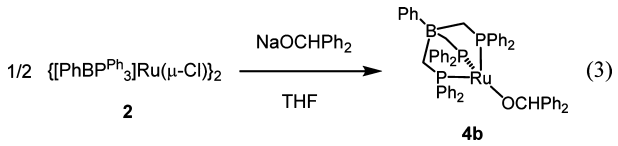

confirmed that it is the same species observed as the possible resting state for catalysis with $EtMe_2SiH$. The ^1H NMR spectrum of **4b** (in C_6D_6) displayed a broad resonance for the alkoxide C−H bond, and this resonance was observed at slightly different chemical shifts depending on the concentration of the solution (^1H δ 6.52 ppm at 70 mM; δ 6.56 ppm at 10 mM), suggesting that **4b** might exist in solution as a monomer−dimer equilibrium. Complex **4a** was previously found to be monomeric in the solid state (by single crystal X-ray diffraction analysis),[9] and it has now been confirmed that **4a** is also primarily monomeric in solution as evident from a molecular weight determination using the Signer method (Expected MW = 859.74 g/mol; found MW = 952 ± 95 g/mol in Et_2O).[12] The solution molecular weight of **4b** could not be determined by this method since **4b** exhibits partial decomposition within 3 h in solution (by ^1H NMR spectroscopy), but the similarity of its $^{31}P\{^1H\}$ NMR data to that of **4a** suggests that **4b** is also primarily monomeric in solution. Treatment of an orange solution of **4b** (in C_6D_6) with $EtMe_2SiH$ (12 equiv) results in a fading of the orange color to yellow within 1 min, and quantitative formation of **3-d_6** and $EtMe_2Si{-}O{-}CHPh_2$ (by ^1H and $^{31}P\{^1H\}$ NMR spectroscopy, eq 4). This establishes that **4b** can react with $EtMe_2SiH$ rapidly enough to account for the observed catalytic hydrosilation of benzophenone with $EtMe_2SiH$.

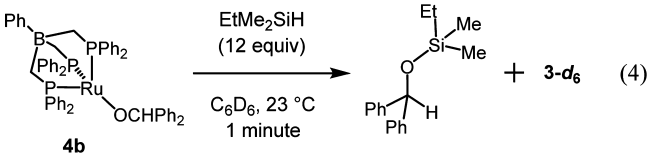

It seemed possible that the hydrosilation of benzophenone with secondary silanes $PhMeSiH_2$ and Ph_2SiH_2 proceeds by a mechanism similar to that proposed for $EtMe_2SiH$. However, the ^1H and $^{31}P\{^1H\}$ NMR spectra of the reaction solutions indicated that **4b** was not the catalyst resting state with these secondary silanes as substrates. Instead, the ^1H NMR spectra of the reaction solutions (in C_6D_6) displayed a new Ru−H resonance (^1H δ −6.03 ppm using $PhMeSiH_2$; ^1H δ −5.60 ppm using Ph_2SiH_2), but the $^{31}P\{^1H\}$ NMR spectra of the reaction solutions contained no observable resonances. These hydride complexes were also formed by stoichiometric reaction of **1a**,**b** with benzophenone (1 equiv in C_6D_6 or CD_2Cl_2), and are identified as silane σ-complexes of the type $[PhBP^{Ph}_3]Ru(H)(\eta^2\text{-}H{-}SiRR'OCHPh_2)$ (RR′ = MePh, **5a**; RR′ = Ph_2, **5b**; eq 5). For the stoichiometric reactions, complexes **5a**,**b** were formed in high yield (ca. 90% by ^1H NMR spectroscopy), and small amounts (ca. 10%) of $RR'HSi{-}O{-}CHPh_2$, **3-d_6** (in C_6D_6), and **4b** were also observed as products (by ^1H and $^{31}P\{^1H\}$ NMR spectroscopy). Complexes **5a**,**b** are unstable to decomposition or reaction with benzophenone (see below),

dx.doi.org/10.1021/ja509073c | J. Am. Chem. Soc. XXXX, XXX, XXX−XXX

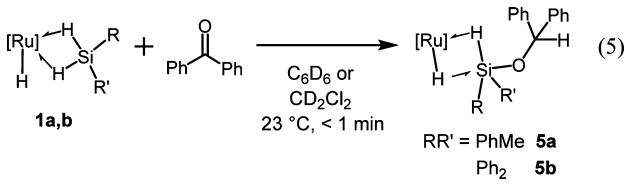

(5)

and these processes may be responsible for formation of the minor products that were observed.

Complex **5a** was also formed by treatment of [PhBP$^{Ph}_3$]Ru-(O^{t}Bu) (**4a**) with the isolated hydrosilation product PhMeHSi−O—CHPh$_2$ (4 equiv) in CD_2Cl_2 (eq 6; note that

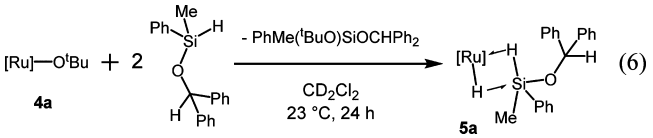

(6)

only 2 equiv of alkoxysilane are consumed, but that an excess was used to increase the reaction rate). In this reaction, one equiv of PhMeHSi−O—CHPh$_2$ is consumed by reaction with **4a** to form PhMe(Ph$_2$HCO)Si−O—^{t}Bu (observed by ^{1}H NMR spectroscopy) and [PhBP$^{Ph}_3$]RuH, which is then trapped by PhMeHSi−O—CHPh$_2$ to form **5a**. Since this route to **5a** starts with the fully formed hydrosilation product PhMeHSi−O—CHPh$_2$, it supports the possibility that **5a,b** are Si−H σ-complexes of the hydrosilation products bound to the [PhBP$^{Ph}_3$]RuH fragment. Complexes **5a,b** were unstable to decomposition (see below), and this prevented isolation of these potential intermediates.

Additional evidence for the identity of **5a,b** was obtained by multinuclear NMR experiments. The presence of Ru−H—Si bonding in **5a,b** is evident from ^{29}Si−^{1}H *J*-coupling observed in the ^{29}Si-filtered ^{1}H and ^{29}Si−^{1}H HMBC NMR spectra of samples generated *in situ* in CD_2Cl_2 (^{1}H δ −6.39 ppm, ^{29}Si δ 22 ppm, J_{SiH} = 50 Hz, **5a**; ^{1}H δ −5.97 ppm, ^{29}Si δ 20 ppm, J_{SiH} = 51 Hz, **5b**).[13] The observed J_{SiH} values are time-averaged for two hydride ligands, as is evident from integration of the Ru−H resonances in the ^{1}H NMR spectra for **5a,b**. The presence of only two hydride ligands suggests that the third hydride ligand of **1a,b** had transferred to benzophenone, and this was supported by the ^{1}H NMR spectra of **5a,b** (in CD_2Cl_2), which display resonances for the methine C−H of the −OCHPh$_2$ group (^{1}H δ 6.17 ppm, **5a**; 6.40 ppm, **5b**). Additionally, this C−H signal exhibits weak *J*-coupling to the ^{29}Si resonance (J_{SiH} < 3 Hz, by ^{1}H−^{29}Si HMBC NMR), and this is consistent with the 3-bond coupling for an Si−O—C−H moiety.[14] This C−H resonance is not observed in the ^{1}H NMR spectrum for a deuterium labeled sample [PhBP$^{Ph}_3$]Ru(D)(η^2-D—SiMePh(OCDPh$_2$)) (**5a-*d*$_3$**) prepared from [PhBP$^{Ph}_3$]-RuD(η^3-D$_2$SiMePh) (**1a-*d*$_3$**), and this provides confirmation that this C−H bond is derived from one of the hydrides of **1a**.

Additional information about the identity of **5a** was obtained from variable temperature NMR experiments on a solution of **5a** (prepared *in situ* in CD_2Cl_2). Notably, in the ^{1}H NMR spectra, the Ru−H resonance exhibits coalescence at −30 °C and at −80 °C there are four Ru−H resonances observed (^{1}H δ −6.12, −6.54, −6.93, −7.38 ppm, Figure 1a). These four observed resonances were determined to actually correspond to six total Ru−H resonances, some of which are overlapping. The ^{1}H{^{31}P} NMR spectrum (−80 °C) revealed that the apparent Ru−H resonance observed at −6.12 ppm (by ^{1}H NMR

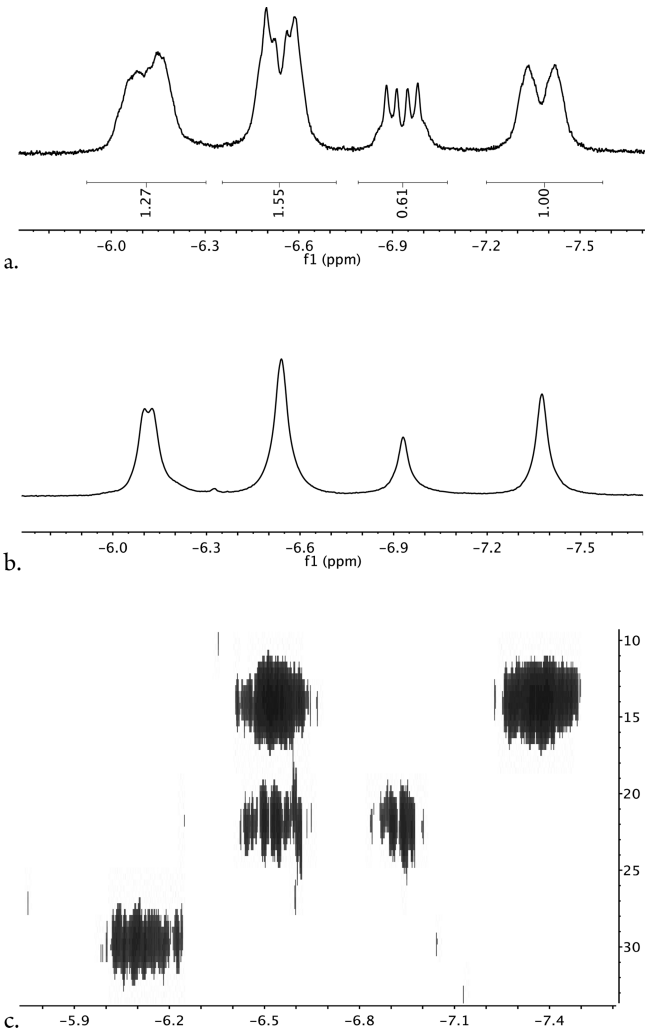

Figure 1. Upfield ^{1}H NMR region (−5.7 to −7.7 ppm) for **5a** collected at −80 C. (a) ^{1}H NMR spectrum. Note that the integral for the most upfield resonance was arbitrarily chosen as 1 H. (b) ^{1}H{^{31}P} NMR spectrum. (c) ^{29}Si−^{1}H HMBC NMR spectrum.

spectroscopy) consists of two closely overlapping resonances of equal height (^{1}H{^{31}P} δ −6.10, −6.14 ppm, Figure 1b). The Ru−H resonance observed at −6.54 ppm (by ^{1}H NMR spectroscopy) also appears to correspond to two different Ru−H resonances that happen to overlap. This is evident from the ^{29}Si−^{1}H HMBC NMR spectrum (−80 °C, Figure 1c), which displays this Ru−H resonance as coupled to two different ^{29}Si NMR resonances (^{29}Si δ 14, 22 ppm; ^{1}H δ −6.54 ppm). Note that the coupling of an *apparent* Ru−H resonance to two different ^{29}Si resonances could also indicate the presence of a ruthenium complex possessing two inequivalent silicon centers, but this possibility is ruled out by the high yield for the formation of **5a** from **1a**, which possesses only one silicon. A total of three ^{29}Si NMR resonances were observed and each couples to a different pair of Ru−H resonances (^{29}Si δ 14 ppm, ^{1}H δ −6.54, −7.38 ppm; ^{29}Si δ 22 ppm, ^{1}H δ −6.54, −6.93 ppm; ^{29}Si δ 30 ppm; ^{1}H δ −6.10, −6.14 ppm). These data are consistent with the presence of three different isomers of **5a** that each feature two inequivalent Ru−H—Si linkages.

The three observable conformational isomers of [PhBP$^{Ph}_3$]-Ru(H)[η^2-H−SiMePh(OCHPh$_2$)] (**5a**) may arise from different rotational conformations of the SiMePh(OCHPh$_2$) group

dx.doi.org/10.1021/ja509073c | J. Am. Chem. Soc. XXXX, XXX, XXX−XXX

(**5a-i**, **5a-ii**, **5a-iii**, eq 7). Computational model isomers of **5a-i** and **5a-ii** (with the $OCHPh_2$ group replaced by $OCHMe_2$)

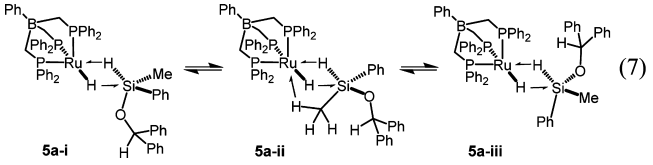

(7)

were examined by DFT geometry optimization calculations and are predicted to be very similar in energy (**5a-i-DFT** and **5a-ii-DFT**, ΔG_{DFT} = −0.66 kcal/mol, Figure 2).[15] The higher energy

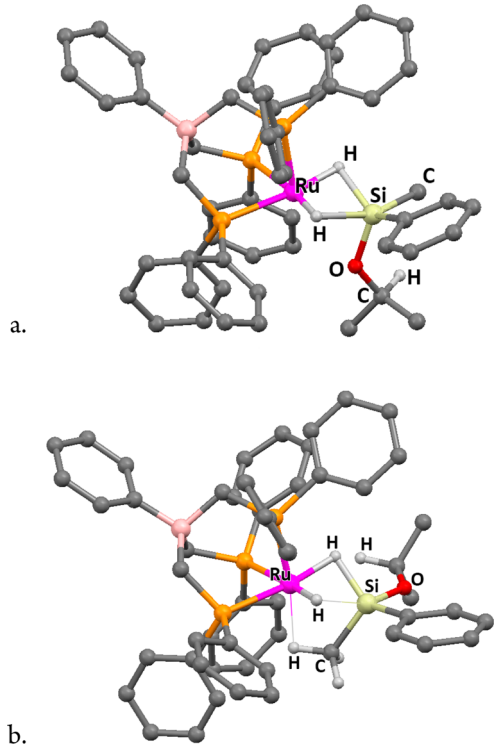

Figure 2. DFT models for isomers of the intermediate **5a**. Note that the $OCHPh_2$ group was truncated to O^iPr. (a) **5a-i-DFT**. (b) **5a-ii-DFT**. Note that the agostic C−H → Ru interaction and the relatively weak Ru−H → Si interaction are indicated by narrow lines.

isomer (**5a-i-DFT**) features two similar Ru−H—Si interactions (d_{Si-H} = 1.89, 2.01 Å; d_{Ru-H} 1.64, 1.63 Å), while these interactions are highly unsymmetrical for the other isomer (d_{Si-H} = 1.71, 2.27 Å; d_{Ru-H} 1.70, 1.63 Å; **5a-ii-DFT**). This latter isomer also features an agostic interaction between ruthenium and a C−H bond of the $Si-CH_3$ group (d_{Ru-H} = 2.14 Å, **5a-ii-DFT**).

Notably, for **5a-ii-DFT**, the corresponding isomer of **5a** (**5a-ii**, eq 7) could be identified by the presence of an upfield ^1H NMR resonance (at −80 °C) that displays coupling to an upfield ^{13}C NMR resonance in the $^{13}C-^1H$ HSQC spectrum (^1H δ −2.73 ppm, ^{13}C δ −50.3 ppm). This ^1H NMR resonance integrates in a 3:1 ratio with the Ru−H peak observed at −7.38 ppm (by ^1H NMR spectroscopy, −80 °C), and this is consistent with the agostic C−H bond being part of a $Si-CH_3$ group, with rapid exchange between all three C−H positions. Notably, the agostic C−H interaction completes an 18 electron count for the ruthenium center, and this would seem to preclude the presence of additional ligands bound to the ruthenium center. As a result, these NMR data provide strong support for the identity of **5a** even though this species could not be isolated and fully characterized.

A second $Si-CH_3$ resonance in the ^1H NMR spectrum of **5a** (δ −0.59 ppm) integrates in a 3:1 ratio with another Ru−H resonance (^1H δ −6.93 ppm), and these two resonances exhibit coupling to the same ^{29}Si nucleus in the $^{29}Si-^1H$ HMBC NMR spectrum (^{29}Si δ 22 ppm, Figure 1c, see Supporting Information for expanded spectrum that includes the $Si-CH_3$ resonance). Note that for each of the two observed $Si-CH_3$ resonances (^1H δ −0.59, −2.73 ppm), there should be two corresponding Ru−H resonances (i.e., a total of four Ru−H resonances for the two isomers), and that the overlapping Ru−H resonances observed at −6.54 ppm (by ^1H NMR spectroscopy) integrate appropriately to correspond to the remaining two expected Ru−H resonances (i.e., the ^1H NMR signal at −6.54 ppm integrates as equal to the sum of the integrals for the ^1H NMR resonances at −6.93 and −7.38 ppm, Figure 1a). The $Si-CH_3$ resonance expected for the third isomer of **5a** could not be located in the ^1H NMR spectrum, and this might be due to overlap of this methyl signal with other resonances in the 0.7−1.8 ppm region of the ^1H NMR spectrum.

Complexes **5a**,**b** are unstable in solution and decompose within 12 h (by ^1H and $^{31}P\{^1H\}$ NMR spectroscopy) to provide the hydrosilation products $RR'HSi-O—CHPh_2$ in quantitative yield (Scheme 4). Complex **3-d_6** was the major

Scheme 4. Comparison of the Reactivity of 5a and 5b

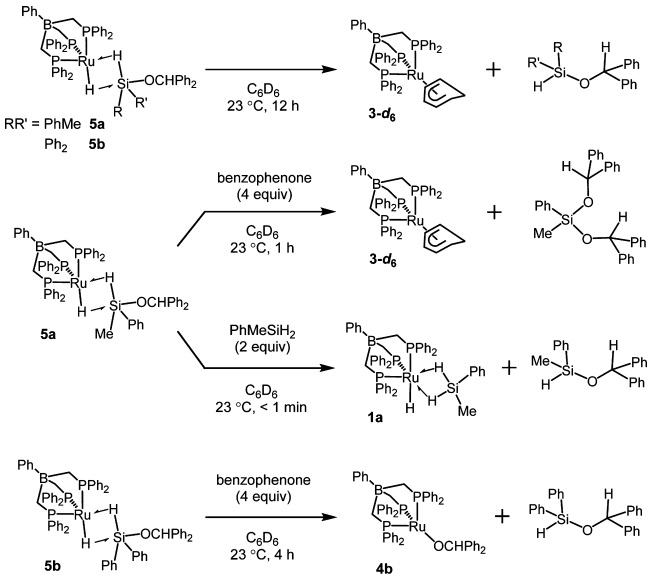

organometallic product of **5a**,**b** decomposition in C_6D_6, and this indicates that loss of the silane product generates a reactive $[PhBP^{Ph}_3]Ru-H$ species that then undergoes addition to the C_6D_6 solvent. Notably, complexes **5a**,**b** react with excess benzophenone (4 equiv, Scheme 4) to give distinctly different products. Treatment of **5a** with benzophenone results in nearly complete consumption of **5a** after 1 h and formation of **3-d_6** in 95% yield, along with the dialkoxysilane hydrosilation product $PhMeSi(OCHPh_2)_2$ (by ^1H NMR spectroscopy). This latter product appears to result from reaction of the initial hydrosilation product $PhMeHSiOCHPh_2$ with **4b** (formed after displacement of $PhMeHSiOCHPh_2$ by benzophenone). Consistent with this possibility, the reaction of **5b** with

dx.doi.org/10.1021/ja509073c | J. Am. Chem. Soc. XXXX, XXX, XXX−XXX

benzophenone resulted in the formation of **4b** and the hydrosilation product $Ph_2HSiOCHPh_2$ after 4 h (by ^1H NMR spectroscopy). Thus, it appears that the hydrosilation product may be displaced from ruthenium by an associative mechanism involving the binding of benzophenone to **5a**,**b** prior to dissociation of the product. The subsequent formation of **4b** is consistent with a hydrosilation mechanism that is analogous to that for tertiary silanes, in which the C−H bond forming step involves insertion of the carbonyl group into a reactive Ru−H bond to generate an alkoxy complex as a key intermediate.

Additional experiments suggest that the hydrosilation mechanism for secondary silanes is distinct from that of tertiary silanes. First, complex **5a** reacts much more rapidly with $PhMeSiH_2$ (2 equiv, <1 min, Scheme 4) than with benzophenone, and this regenerates the η^3-$H_2SiMePh$ complex **1a** in quantitative yield. Furthermore, stoichiometric reactions of **4b** with secondary silanes (Scheme 5) rule out the possibility

Scheme 5. Reactions of 4b with Secondary Silanes

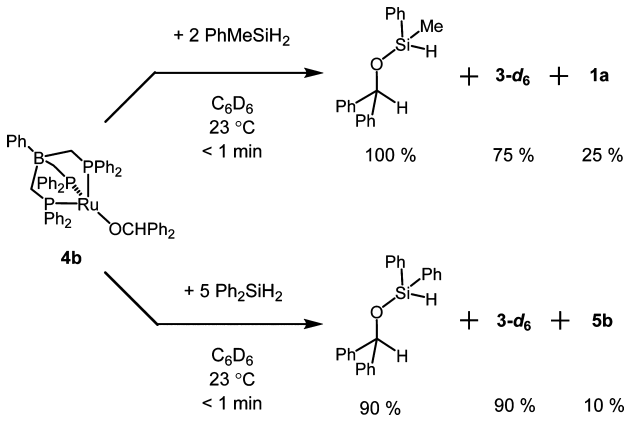

that **4b** is an intermediate in the catalytic hydrosilation reactions using $PhMeSiH_2$ or Ph_2SiH_2. Treatment of **4b** with $PhMeSiH_2$ (2 equiv in C_6D_6) results in an immediate color change from orange to yellow and formation of the expected silyl ether in quantitative yield. Complex **3-d_6** was the major organometallic product (75%) and **1a** was observed as a minor product (25%). The treatment of **4b** with Ph_2SiH_2 (5 equiv) provided similar results (90% yield of $Ph_2HSiOCHPh_2$ and **3-d_6**), except that **5b** was formed as the minor product (10%) rather than **1b**. Thus, reactions of secondary silanes with **4b** represent an effective route for the formation of hydrosilation products, but these results demonstrate that this pathway would result in rapid deactivation of the catalyst in C_6D_6 by the formation of **3-d_6**. Since the rapid formation of **3-d_6** was not observed under catalytic conditions for most substrates, an alternate mechanism must be considered to account for the high turnover numbers for catalysis with secondary silanes.

Mechanistic Investigation by Kinetic analyses. The hydrosilation of benzophenone using $PhMeSiH_2$ (in CD_2Cl_2) was monitored by ^1H NMR spectroscopy at −18 °C using **1a** as the catalyst. At this temperature, both **5a** and **1a** were observed (by ^1H NMR spectroscopy) within 1 min of mixing the reactants, whereas only **5a** was observed as a resting state for catalytic reactions examined at 23 °C. Interestingly, the ^1H NMR resonance for the Ru−H groups of **1a** (δ −7.26 ppm in CD_2Cl_2 at −18 °C) shifts slightly upfield (to ca. δ −7.5 ppm) immediately after the addition of benzophenone (typical concentrations of 0.15−0.20 M) to a solution of **1a** and $PhMeSiH_2$. Over the course of the reaction, the Ru−H resonance for **1a** moves steadily downfield, and returns to its normal value upon complete consumption of benzophenone. Additionally, with a much larger loading of benzophenone (0.70 M) the Ru−H resonance was observed even further upfield (^1H δ −8.08 ppm). This apparent dependence of the Ru−H chemical shift of **1a** on the concentration of benzophenone suggests that this resonance might result from a rapid interconversion of **1a** and its benzophenone adduct $[PhBP^{Ph}_3]Ru(\mu\text{-}H)_3Si(MePh)\leftarrow O{=}CPh_2$ (**1a(O=CPh$_2$)**), eq 8). Note that a similar concentration-dependent perturba-

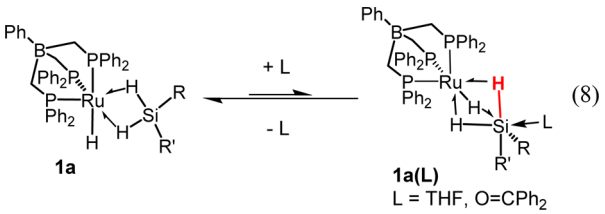

(8)

tion of the Ru−H resonances of **1a** has previously been observed as a consequence of equilibration between **1a** and a weakly associated THF adduct, **1a(THF)** (eq 8).[8] Unfortunately, **1a(O=CPh$_2$)** could not be more clearly identified due to the weak binding of benzophenone to **1a,** and the rapid conversion of **1a(O=CPh$_2$)** to **5a**.

Interestingly, **1a** and **5a** were simultaneously observed (by ^1H NMR spectroscopy) during catalytic reactions monitored at −18 °C. The ratio of the concentrations of these ruthenium species was dependent on the relative concentrations of the substrates $PhMeSiH_2$ and benzophenone. With a large initial excess of benzophenone (5 equiv relative to $PhMeSiH_2$), the initial concentration of **5a** was ca. 6 times larger than that of **1a** (determined by ^1H NMR spectroscopy). Conversely, an initial excess of $PhMeSiH_2$ (5 equiv relative to benzophenone) resulted in observation of a larger concentration of **1a** (ca. 5 times more **1a** than **5a**). Thus, the ratio [**1a**]:[**5a**] appears to be directly proportional to the $[PhMeSiH_2]$:$[O{=}CPh_2]$ ratio. Further support for this possibility was obtained by monitoring catalytic reactions starting with other initial ratios of the substrates (e.g., initial $[PhMeSiH_2]$:$[Ph_2C{=}O]$ ratios of 17:10, 10:11, and 10:15, see Supporting Information). However, the low concentrations of each ruthenium species and the broadness of the Ru−H resonances prevented precise integration of the Ru−H resonances for **1a** and **5a**. Thus, the exact quantitative dependence of the ratio [**1a**]:[**5a**] on the concentration of the reactants could not be definitively established.

Given the dependence of the [**5a**]:[**1a**] ratio on the ratio of $[Ph_2C{=}O]$ to $[PhMeSiH_2]$, the kinetics of the reaction were examined by ^1H NMR measurements (at −18 °C) using 5:1 and 1:5 initial ratios of the reactants (Figure 3). Under conditions of excess benzophenone, complex **5a** was the major $[PhBP^{Ph}_3]Ru$ species observed (85−100% of $[PhBP^{Ph}_3]Ru$ by ^1H NMR spectroscopy), and the reaction exhibited first order dependence on the concentration of the limiting reactant $PhMeSiH_2$ (Figure 3a). Under these conditions, the reaction was also determined to exhibit first order dependence on the concentration of **5a** (Figure 3a), and thus an overall second-order rate law was determined (eq 9). In contrast, under conditions of excess $PhMeSiH_2$, the Ru−H resonance for **1a** was observed to account for >85% of $[PhBP^{Ph}]Ru$ present (by

dx.doi.org/10.1021/ja509073c | J. Am. Chem. Soc. XXXX, XXX, XXX−XXX

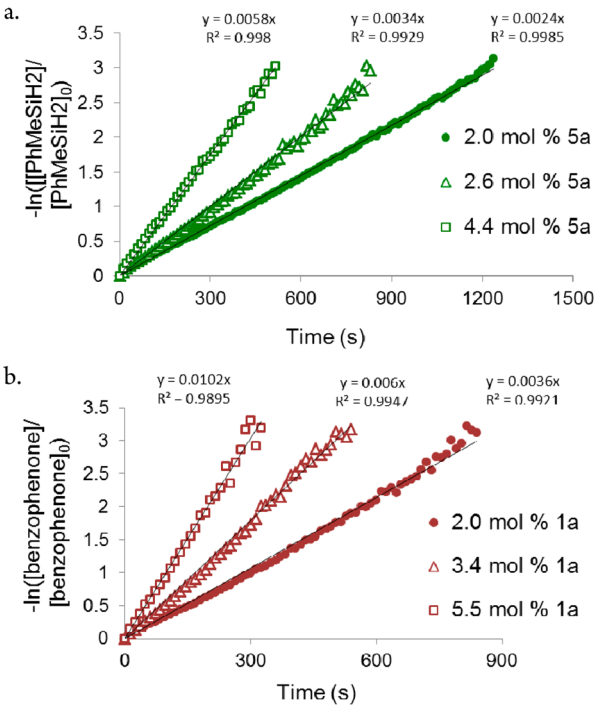

Figure 3. Kinetic data from catalytic hydrosilation reactions. (a) Plots of $-\ln([PhMeSiH_2]/[PhMeSiH_2]_0)$ versus time for 3 different catalyst loadings and excess benzophenone (5 equiv). (b) Plots of $-\ln([benzophenone]/[benzophenone]_0)$ versus time for 3 different catalyst loadings and an excess of $PhMeSiH_2$ (5 equiv).

^{1}H NMR spectroscopy), and the reaction was found to exhibit first order dependence on the concentration of benzophenone and **1a** (second order overall, Figure 3b and eq 10). Note that eqs 9 and 10 could conceivably result from pseudo-first-order simplifications of a third-order rate law involving both substrates (i.e., $d[P]/dt = k''_{obs}[PhMeSiH_2][Ph_2CO][Ru]$), but this possibility was eliminated by an additional experiment using nearly equal amounts of each substrate (initial $[PhMeSiH_2]$:$[Ph_2C{=}O]$ ratio of 10:11; see Supporting Information).

$$\frac{d[P]}{dt} = k_{obs}[PhMeSiH_2][\mathbf{5a}] \quad (9)$$

$$\frac{d[P]}{dt} = k'_{obs}[Ph_2CO][\mathbf{1a}] \quad (10)$$

The observation of two apparent catalyst resting states (**1a** and **5a**) and the determination of two distinct rate laws (eqs 9 and 10) indicate that the catalytic cycle includes two steps that are similar in energy, such that either step can be rate limiting depending on the ratios of the reactants used. Thus, the two rate laws that were determined provide information about two distinct steps in the catalytic cycle, and these rate laws are consistent with the catalytic cycle depicted in Scheme 6. This mechanism starts with the binding of benzophenone to the silicon center of $[PhBP^{Ph}_3]RuH(\eta^3\text{-}H_2SiMePh)$ (**1a**) to form the adduct **1a(O═CPh$_2$)**. This facilitates a 1,2-insertion of the carbonyl group into the Si−H portion of an Ru−H—Si 3c−2e bond, to form the observed intermediate **5a**. If the 1,2-insertion step is rate-limiting for the catalytic cycle, then applying the steady state approximation to the concentration of **1a(O═CPh$_2$)** provides the rate law depicted in eq 10. However, at high concentrations of benzophenone relative to $PhMeSiH_2$, the 1,2-insertion step appears to occur rapidly enough that the rate limiting step becomes displacement of the product silane ($PhMeHSi{-}O{-}CHPh_2$) from **5a** by the reactant silane ($PhMeSiH_2$) to regenerate **1a**, and the rate law becomes that of eq 9. The rate dependence on $k'_{obs}[\mathbf{5a}][PhMeSiH_2]$ (eq 9) indicates that the binding of $PhMeSiH_2$ to **5a** assists in displacement of the product from ruthenium, and this associative pathway for product/silane exchange avoids the formation of the free 14 electron $[PhBP^{Ph}_3]Ru{-}H$ species that could be responsible for undesired side reactions (e.g., formation of **3-d_6** in C_6D_6). Thus, this mechanism explains why catalysis occurs for the secondary silanes in C_6D_6, but not for tertiary silanes, which cannot lead to the formation of intermediates analogous to **5a,b**.

Scheme 6. Proposed Catalytic Cycle for Hydrosilation of Benzophenone with $PhMeSiH_2$ and 1a as a Catalyst

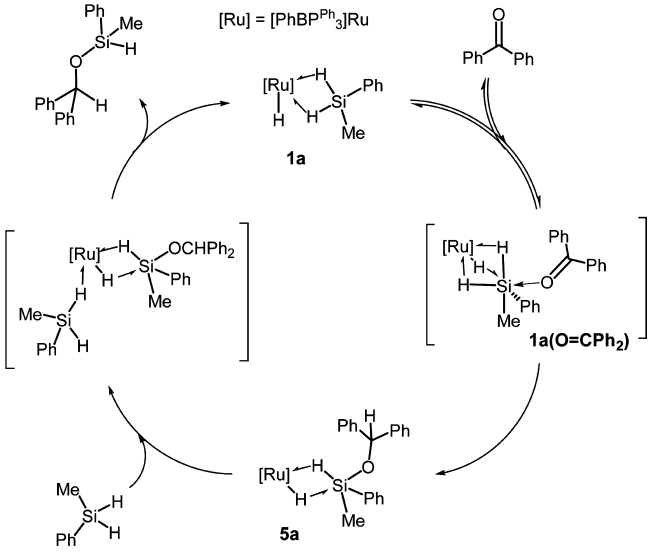

Computational Investigation of the Catalytic Cycle. The proposed catalytic cycle was examined by DFT calculations on the hydrosilation of acetone with $PhMeSiH_2$ (Scheme 7).[15] A DFT model of the complete structure of **1a** (**1a-DFT**, $G_{\text{1a-DFT}} = 0$) was used as the starting point for the catalytic cycle. The binding of acetone to the silicon center of **1a-DFT** to form the adduct **1a-ace-DFT** is predicted to be endergonic, but only by a small amount ($\Delta G_{\text{1a-aceDFT}} = +5.1$ kcal/mol). This is consistent with the experimental observation that the ^{1}H NMR chemical shift for the Ru−H resonance of **1a** exhibits small changes depending on the concentration of benzophenone, which suggests an equilibrium between **1a** and a weakly bound benzophenone adduct **1a(O═CPh$_2$)**. For **1a-ace-DFT**, the Si−O—C angle is wider than expected for an sp^2 or sp^3 hybridized oxygen (Si−O—C angle = 138.19°, Figure 4a). In contrast, other Lewis bases (i.e., DMAP, PMe_3, XylNC)[8,9] bind to the silicon center of **1a,b** with a more ideal geometry about the donor atom (for example, **1b(DMAP)** exhibits Si−N−C angles of 120.2(2)° and 123.8(2)° for the sp^2 hybridized donor nitrogen).[8] The wide Si−O−C angle for **1a-ace-DFT** might be due to unfavorable steric interactions between the acetone methyl groups and the $[PhBP^{Ph}_3]^-$ ligand. Additionally, one of the Si−H distances in **1a-ace-DFT** is relatively long (d_{Si-H} = 2.20, 1.83, 1.91 Å), whereas related base adducts exhibit three Ru−H—Si interactions with roughly equivalent bond distances.[8,9] This difference may be due to weak binding of the

dx.doi.org/10.1021/ja509073c | J. Am. Chem. Soc. XXXX, XXX, XXX−XXX

Scheme 7. Catalytic Cycle Determined by DFT Calculations for the Hydrosilation of Acetone Using 1a

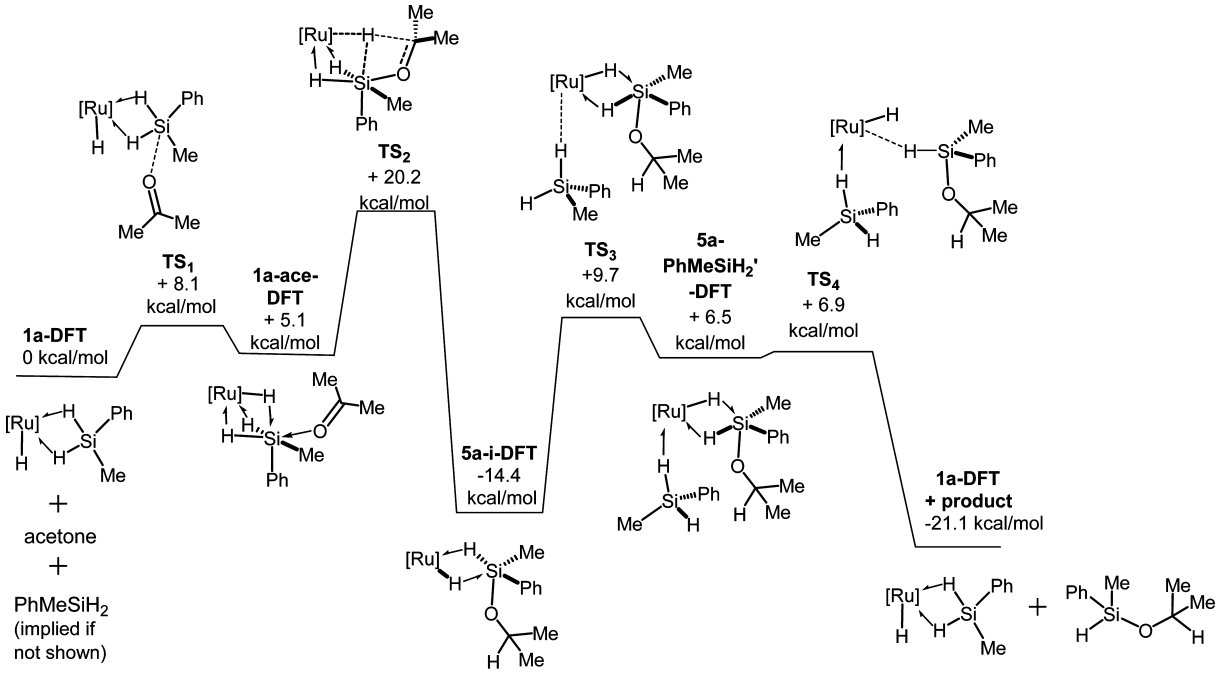

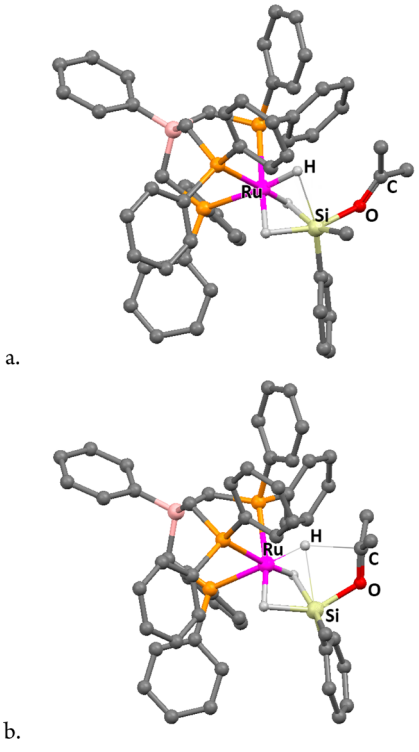

Figure 4. (a) Structure of the model acetone adduct **1a-ace-DFT** determined by DFT structure optimization. Note that the comparatively weak Ru−H → Si interaction is indicated with a narrow bond line. (b) Transition state for the C−H bond forming step of the catalytic cycle (**TS$_2$**). Bonds that are breaking or forming are depicted with narrow lines. Note that for both structures, the non-hydridic hydrogens have been omitted for clarity.

ketone relative to stronger Lewis bases, such that a stronger resemblance to the initial η^3-H_2SiMePh complex is preserved in the acetone adduct.[16] Note that the longest Si−H distance for **1a-ace-DFT** is too long to correspond to a σ-H−Si ligand, but still indicates the presence of a weak Ru−H → Si interaction to provide silicon with a coordination number of 6.[17,13b]

A transition state for C−H bond formation was determined to have an energy barrier that is readily accessible at room temperature (ΔG_{TS2} = 20.2 kcal/mol). At this transition state, all of the Si−H distances have increased (d_{Si-H} = 2.33, 2.06, 1.88 Å, Figure 4b), with the longest Si−H distance corresponding to the hydride that is transferred to the carbonyl group. Thus, at the transition state, the Si−H interaction associated with the migrating hydrogen is nearly completely broken,[17,13b] and this transition state resembles those expected for transfer of a terminal metal hydride to a ketone that is bound to a silylene ligand.[4,6] The silicon center has moved away from the central axis of the [$PhBP^{Ph}_3$]Ru moiety (B−Ru—Si angle = 166.6°, **TS$_2$**; 173.2°, **1a-ace-DFT**), and the O=CMe_2 group has rotated so that oxygen appears to be bound to silicon through the C=O π-bond rather than via an oxygen lone pair (Si−O—C−C dihedral angles = 85.64°, 116.0°, **TS$_2$**). This positions the carbonyl group for accepting the hydride, but the Ru−H distance is not significantly elongated at the transition state (d_{Ru-H} = 1.63 Å, **1a-ace-DFT**; d_{Ru-H} = 1.70 Å, **TS$_2$**), and the C−H distance has decreased considerably but is still fairly long (3.44 Å, **1a-ace-DFT**; d_{C-H} = 1.99 Å, **TS$_2$**). Thus, it appears that the energetic cost for H-migration derives primarily from the repositioning of acetone to accept the hydride, and that flexibility of the [(μ-$H)_3$SiMePh(O=CMe_2)] moiety allows this to occur with a fairly low barrier. The transfer of the hydride ligand occurs without a significant perturbation to the other two Ru−H−Si interactions, and this results in the ready formation of **5a-i-DFT**. Thus, activation of the ketone at silicon ultimately accounts for the experimentally observed formation of **5a**,**b** as key intermediates in the hydrosilation of benzophenone with $PhMeSiH_2$ or Ph_2SiH_2.

A transition state for the addition of $PhMeSiH_2$ to **5a-i-DFT** was found to be associated with an energy barrier ($\Delta\Delta G_{TS3-5a-i-DFT}$ = +24.1 kcal/mol) that is higher than that

dx.doi.org/10.1021/ja509073c | J. Am. Chem. Soc. XXXX, XXX, XXX−XXX

for the hydride transfer, but only by a small amount (3.9 kcal/mol). Interestingly, the addition of $PhMeSiH_2$ to **5a-i-DFT** forms an η^1-H−SiHMePh complex (Ru−H−Si angle = 169.8°, **5a-PhMeSiH$_2$-DFT**), which minimizes steric crowding for this intermediate. A transition state for dissociation of the product from **5a-PhMeSiH$_2$-DFT** could not be located after several attempts at transition state optimization calculations starting from slightly different initial geometries. Instead, a transition state was located for product dissociation from a slightly higher energy diastereomer of **5a-PhMeSiH$_2$-DFT** (**5a-PhMeSiH$_2$′-DFT**, $\Delta\Delta G_{\mathbf{5a'\text{-}PhMeSiH2'\text{-}DFT-5a'\text{-}PhMeSiH2\text{-}DFT}}$ = +2.4 kcal/mol), and this transition state is associated with a very low barrier ($\Delta\Delta G_{\mathbf{TS4\text{-}5a'\text{-}PhMeSiH2'\text{-}DFT}}$ = +0.4 kcal/mol). Note that a transition state analogous to **TS$_3$**, but leading to the formation of **5a-PhMeSiH2′-DFT** (**TS$_{3'}$**), was not calculated since it could be readily estimated that this transition state would be no more than 2.4 kcal/mol higher in energy than **TS$_3$**, and that **TS$_{3'}$** would be very similar in geometry to **TS$_3$**. After dissociation of the hydrosilation product, rearrangement of [PhBP$^{Ph}_3$]RuH(η^2-HSiHMePh) should occur very rapidly to regenerate the η^3-H_2SiMePh complex **1a**, and this step was not examined computationally. Note that the two highest energy barriers in the computationally determined catalytic cycle are associated with reaction steps that are consistent with the two experimentally determined rate laws for the hydrosilation of benzophenone with $PhMeSiH_2$ (eqs 9 and 10). Thus, the accuracy of the computationally determined catalytic cycle is bolstered by its consistency with experimental observations made for the catalytic ketone hydrosilation reactions.

CONCLUSION

The electrophilic η^3-H_2SiRR′ σ-silane complexes **1a**,**b** are effective hydrosilation catalysts for a variety of ketone substrates. Complex **1a** was a particularly efficient catalyst for the hydrosilation of benzophenone with $PhMeSiH_2$, which could be accomplished with high turnover rates and overall turnover numbers. Interestingly, detailed mechanistic investigations revealed that there are two distinct catalytic cycles available for these carbonyl hydrosilation reactions depending on the silane substrate that is used (i.e., secondary or tertiary silanes), but that the two pathways provide similar reaction rates (i.e., within 1 order of magnitude at room temperature).

For the hydrosilation of benzophenone with $EtMe_2SiH$, the mechanism involves insertion of benzophenone into the Ru−H bond of a highly reactive ruthenium hydride species to generate [PhBP$^{Ph}_3$]Ru−OCHPh$_2$ (**4b**), which was observed as the resting state of the catalytic cycle (by $^{31}P\{^1H\}$ NMR spectroscopy). Complex **4b** was isolated and this species was found to react rapidly with $EtMe_2SiH$ to form $EtMe_2SiOCHPh_2$ and regenerate the reactive ruthenium hydride species. This hydrosilation mechanism is analogous to the Chalk−Harrod mechanism for catalytic olefin hydrosilations,[18] and similar mechanisms have previously been proposed for catalytic carbonyl hydrosilation reactions involving tertiary silanes.[19] However, mechanistic studies on several hydrosilation catalysts have revealed that this mechanism is often a minor hydrosilation pathway, and that other, more active catalytic cycles are responsible for the majority of catalysis.[20] Thus, it is notable that **4b** reacts with $EtMe_2SiH$ rapidly enough to confirm that the Chalk-Harrod type pathway is primarily responsible for the hydrosilation of benzophenone with $EtMe_2SiH$ when using **1a** as a precatalyst.

Interestingly, experimental and computational results indicate that an entirely different mechanism is responsible for hydrosilation with secondary silanes. These reactions proceed via binding of the ketone substrate to the electrophilic silicon center of the η^3-H_2SiRR′ ligand in **1a**,**b**, followed by transfer of a hydride to the ketone. These hydrosilation reactions are the first catalytic reactions to be identified as involving electrophilic η^3-H_2SiRR′ ligands, and it is interesting that these Si−H σ-complexes mediate hydrosilation by a mechanism that differs considerably from the mechanisms proposed for electrophilic η^1- and η^2-H−SiR_3 σ-complexes, whereby the coordinated Si−H bond is cleaved upon attack of the ketone substrate at silicon.[5,7b] Instead, the mechanism for the catalysts **1a**,**b** more closely resembles catalytic cycles that propose the involvement of electrophilic silylene complexes that form distinct L_nMH-(SiRR′←ketone) intermediates prior to the C−H bond forming step.[4,6]

The catalytic cycle for **1a**,**b** uniquely features a hypercoordinate silicon intermediate (i.e., **1a**,**b**(**O═CRR′**)), and this intermediate leads to insertion of the carbonyl group into a highly polarized Si−H bond that is part of an Ru−H → Si interaction. This step is similar to a 1,2-insertion step that has previously been proposed for the stoichiometric hydrosilation of ketones with hydridosilicate anions (e.g., $[(RO)_4SiH]^-$)[21] or for for catalytic hydrosilation reactions involving M—[SiR_2H-(O═CR′R″)] intermediates.[3] However, the latter mechanistic proposal has received little experimental or theoretical support.[4a] For the present system, the 1,2-insertion step leads to the formation of intermediates **5a**,**b**, in which the product is bound to ruthenium as a σ-silane ligand. This protects the reactive Ru−H bond from detrimental side reactions (e.g., addition to benzene) until a new silane substrate displaces the product. Thus, the η^3-H_2SiRR′ ligands play a crucial role in activating the ketone substrate, and this has the remarkable effect of selecting for a hydrosilation pathway that is more robust than that available to tertiary silanes. Future work will focus on investigating the activation of additional unsaturated substrates by the silicon center of **1a**,**b**, as well as further examining the more general role of how Ru−H—Si interactions might be useful for guiding the catalytic cycle of hydrosilation reactions.

EXPERIMENTAL DETAILS

General Considerations. All manipulations of air sensitive compounds were conducted under a nitrogen atmosphere using standard Schlenk techniques or using a nitrogen atmosphere glovebox. Proteo solvents were dried using a JC Meyer solvent drying system, and deutero solvents were vacuum transferred from appropriate drying agents (NaK for C_6D_6 and CaH_2 for CD_2Cl_2). Silanes were purchased from commercial sources and used as received. Complexes **1a**,**b**,[8] **2**,[22] and **4a**[9] were prepared as previously reported. Diphenylmethanol was prepared based on a published procedure,[23] and was deprotonated using NaH (in THF) to form Na[$OCHPh_2$], which was isolated as a white powder after evaporating the solvent under vacuum.

NMR spectra were recorded on Bruker spectrometers at room temperature unless otherwise noted. Spectra were referenced internally by the residual proton signal relative to tetramethylsilane for ^1H NMR, solvent peaks for $^{13}C\{^1H\}$ NMR, external 85% H_3PO_4 for $^{31}P\{^1H\}$ NMR, and tetramethylsilane for $^{29}Si-^1H$ HMBC experiments. The J_{SiH} values for Ru−H—Si resonances were determined by examining satellite signals near the main Ru−H resonance in $^1H\{^{31}P\}$ NMR spectra or by the Ru−H resonances displayed in ^{29}Si-filtered $^1H\{^{31}P\}$ NMR experiments. Hydrosilation products were identified by comparison of multinuclear NMR data (^1H, $^{13}C\{^1H\}$, and $^{29}Si-^1H$ HMBC NMR) to those previously reported for identical or closely

dx.doi.org/10.1021/ja509073c | J. Am. Chem. Soc. XXXX, XXX, XXX−XXX

related silyl ethers, and by GC−MS. Elemental analyses were performed by the University of California, Berkeley College of Chemistry Microanalytical Facility.

[PhBP$^{Ph}_3$]Ru−OCHPh$_2$ (4b). Complex **2** (62 mg, 0.038 mmol) and Na[OCHPh$_2$] (16 mg, 0.078 mmol) were dissolved in 4 mL of THF and the resulting red solution was stirred for 40 min. After this time, the solution was evaporated under vacuum and the resulting solid was extracted with Et$_2$O (3 mL) to give a brownish-red solution, which was filtered and cooled to −35 °C. After 9 days, a brown crystalline precipitate had formed and the solution was a lighter, purer red color. The supernatant was removed by pipet and evaporated under vacuum to provide **4b** as an analytically pure, red-orange foam (44 mg, 66%). Anal. Calcd for $C_{58}H_{52}OBP_3Ru$ (969.853): C, 71.83; H, 5.40. Found: C, 72.16; H, 5.03. ^{1}H NMR (C$_6$D$_6$, 600 MHz): δ 8.18 (d, J = 7.1 Hz, 2 H), 7.75 (m, 6 H), 7.48 (br, 12 H), 7.28 (t, J = 7.3 Hz, 4 H), 7.11 (t, J = 7.3 Hz, 1 H), 7.02 (t, J = 7.5 Hz, 2 H), 7.73−7.63 (m, 18 H), 6.56 (1 H, RuOCHPh$_2$), 1.61 (br, 6 H, BCH$_2$P). ^{13}C{^{1}H} NMR (C$_6$D$_6$, 150.893 MHz): δ 148.61, 139.22, 138.63, 132.86, 132.44, 132.08, 130.57, 128.96, 128.90, 127.72, 127.47, 125.18, 84.37 (Ru−O−CPh$_2$H), 13.91 (br, BCH$_2$P). ^{31}P {^{1}H} NMR (C$_6$D$_6$, 161.967 MHz): δ 79.0.

***In Situ* Preparation and Observation of 5a,b.** Complexes **5a,b** were prepared by the addition of benzophenone (1 equiv) to solutions of **1a,b** in C$_6$D$_6$ or CD$_2$Cl$_2$. Upon addition of benzophenone, the pale yellow color of **1a,b** darkens to amber yellow. The solutions were examined by ^{1}H, ^{1}H{^{31}P}, ^{31}P{^{1}H}, and ^{29}Si−^{1}H HMBC NMR spectroscopy. Note that **1a**, **3-d_6**, and **4b** were observed as minor species in solutions of **5a,b** prepared in this manner. The ^{31}P{^{1}H} NMR signals for **5a,b** could not be observed for samples at room temperature, presumably as a result of broadening due to conformational changes in solution. At lower temperatures, several new ^{31}P{^{1}H} NMR signals were observed and are consistent with the presence of several conformational isomers of **5a**. Note that the sample of **5a** used for low temperature NMR spectroscopy contained larger impurities of **4b** (ca. 30% of [Ru] present) and PhMeSi(OCHPh$_2$)$_2$ than typical for samples of **5a** prepared *in situ*, but that this did not interfere with obtaining key low temperature NMR data for **5a**. See Figure 1 and the Supporting Information for low temperature NMR spectra. Distinguishing room temperature NMR data are tabulated here.

5a. ^{1}H NMR (CD$_2$Cl$_2$ 500 MHz) δ 7.75 (J_{SiH} < 3 Hz, 2 H, Si−Ph), 6.16 (J_{SiH} < 3 Hz, 1 H, SiOCPh$_2$—H), 1.44 (br, 6 H, BCH$_2$P), −0.56 (3 H, Si−CH$_3$), −6.39 (m, J_{SiH} = 50 Hz, 2 H, Ru−H). ^{29}Si−^{1}H HMBC NMR: ^{29}Si δ 22 ppm.

5b. ^{1}H NMR (CD$_2$Cl$_2$ 600 MHz) δ 6.39 (J_{SiH} < 3 Hz, 1 H, SiOCPh$_2$—H), 1.40 (br, 6H, BCH$_2$P), −5.97 (m, J_{SiH} = 51 Hz, 2 H, Ru−H). ^{29}Si−^{1}H HMBC NMR: ^{29}Si δ 20 ppm.

Representative Procedure for Catalytic Hydrosilation Reactions. Benzophenone (20 mg, 0.11 mmol) and PhMeSiH$_2$ (13.5−16.0 mg, 0.11−0.13 mmol) were dissolved in C$_6$D$_6$ (0.6 mL) with C$_6$Me$_6$ as an internal standard. A ^{1}H NMR spectrum of the mixture was collected prior to adding **1a,b** in C$_6$D$_6$ (0.1 mL). The addition of **1a** produces an amber yellow solution that was examined by ^{1}H NMR spectroscopy within 15 min. It was noted that fading of the amber yellow color to a pale yellow or colorless solution appeared to coincide with complete consumption of benzophenone (determined by ^{1}H NMR). The product was isolated by diluting the reaction solution with hexanes (1 mL), passing this solution through a plug of silica, and evaporating the solvent. This provided the product in good purity (≥95%) judged by ^{1}H NMR spectroscopy. See Supporting Information for NMR spectral data and GC/MS data for all isolated products.

Representative Procedure for Low Temperature Reaction Monitoring and Kinetics Data Collection. Complex **1a** (2.7 mg, 0.003 mmol) and PhMeSiH$_2$ (11 mg, 0.09 mmol) were dissolved in 0.6 mL of a stock solution of CD$_2$Cl$_2$ containing C$_6$Me$_6$ as an internal standard. This solution was transferred to a J-Young NMR tube, which was then charged with a small plastic tube that was packed with solid benzophenone, and the NMR tube was sealed with a threaded Teflon stopper. The plastic inset with benzophenone fits snuggly at the top of the NMR tube, thus keeping the benzophenone substrate separate from the solution. An initial ^{1}H NMR spectrum of the solution was collected at −18 °C (temperature was calibrated by an external standard of 4% MeOH in methanol-d_4). In this initial ^{1}H NMR spectrum, the Ru−H resonance for **1a** is displayed as a sharp signal and the concentration of **1a** was quantified by integration of the Ru−H resonance relative to the resonance for C$_6$Me$_6$. The sample was then chilled in a dry ice/^{i}PrOH bath before briskly shaking the NMR tube to dissolve benzophenone into the solution. The sample was immediately transferred to the NMR probe cooled to −18 °C and allowed 1 min to equilibrate in temperature before collection of ^{1}H NMR spectra at 12 s intervals.

Computational Details. All calculations were performed using the Gaussian '09 suite of programs in the molecular graphics and computing facility of the College of Chemistry, University of California, Berkeley. Calculations were performed using the B3PW91 hybrid functional with the 6-31G(d,p) basis set for all main-group elements and the LANL 2DZ basis set for ruthenium. The full [PhBP$^{Ph}_3$]Ru fragment and SiMePh fragment were used for all calculations. Vibrational frequencies were calculated for all converged structures and confirm that these structures are transition states (one imaginary frequency determined) or lie on minima (no imaginary frequencies were determined). Energies for all species are free energies determined relative to **1a-DFT** + **acetone-DFT** + **PhMeSiH$_2$-DFT**. Only half the entropic contributions to the free energy differences that were determined by DFT calculations were used, which was done as an approximate correction for the determination of dilute gas-phase free energies by DFT calculations rather than solution-state free energies.[24] This results in ca. an 8 kcal/mol decrease in the relative energy of transition states or intermediates (in comparison to the gas phase values) formed in bimolecular processes.

■ ASSOCIATED CONTENT

Ⓢ Supporting Information

Additional experimental and computational details, and NMR spectra. This material is available free of charge via the Internet at http://pubs.acs.org.

■ AUTHOR INFORMATION

Corresponding Author

tdtilley@berkeley.edu

Notes

The authors declare no competing financial interest.

■ ACKNOWLEDGMENTS

This work was funded by the National Science Foundation under Grant No. CHE-1265674. The molecular graphics and computational facility (College of Chemistry, University of California, Berkeley) is supported by the National Science Foundation under Grant No. CHE-0840505. We thank Allegra Liberman-Martin for discussion of kinetics data.

■ REFERENCES

(1) (a) Ojima, I.; Li, Z.; Zhu, J. *The Chemistry of Organic Silicon Compounds*; Wiley: Avon, 1998; Chapter 29. (b) Rappoport, Z.; Apeloig, Y. *The Chemistry of Organic Silicon Compounds*; Wiley: Chichester, U.K., 1998. (c) Roy, A. K. *Adv. Organomet. Chem.* **2007**, *55*, 1−59. (d) Riener, K.; Högerl, M. P.; Gigler, P.; Kühn, F. E. *ACS Catal.* **2012**, *2*, 613−621.

(2) (a) Ojima, I.; Nihonyanagi, M.; Kogure, T.; Kumagai, M.; Horiuchi, S.; Nakatsugawa, K. *J. Organomet. Chem.* **1975**, *94*, 449. (b) Ojima, I.; Kogure, T.; Kumagai, M.; Horiuchi, S.; Sato, T. *J. Organomet. Chem.* **1976**, *122*, 83−97.

(3) Zheng, G. Z.; Chan, T. H. *Organometallics* **1995**, *14*, 70−79.

(4) (a) Schneider, N.; Finger, M.; Haferkemper, C.; Bellemin-Laponnaz, S.; Hofmann, P.; Gade, L. H. *Angew. Chem., Int. Ed.* **2009**, *48*, 1609−1613. (b) Schneider, N.; Finger, M.; Haferkemper, C.; Bellemin-Laponnaz, S.; Hofmann, P.; Gade, L. H. *Chem.—Eur. J.*

2009, *15*, 11515−11529. (c) Gigler, P.; Bechlars, B.; Kühn, F. E. *J. Am. Chem. Soc.* **2011**, *133*, 1589−1596.
(5) (a) Gutsulyak, D. M.; Vyboishchikov, S. F.; Nikonov, G. I. *J. Am. Chem. Soc.* **2010**, *132*, 5950−5951. (b) Park, S.; Brookhart, M. *Organometallics* **2010**, *29*, 6057−6064. (c) Yang, Y.-F.; Chung, L. W.; Zhang, X.; Houk, K. N.; Wu, Y.-D. *J. Org. Chem.* **2014**, *79*, 8856−8864.
(6) (a) Watanabe, T.; Hashimoto, H.; Tobita, H. *J. Am. Chem. Soc.* **2006**, *128*, 2176−2177. (b) Ochiai, M.; Hashimoto, H.; Tobita, H. *Dalton Trans.* **2009**, 1812−1814. (c) Ochiai, M.; Hashimoto, H.; Tobita, H. *Organometallics* **2012**, *31*, 527−530. (d) Mitchell, G. P.; Tilley, T. D. *J. Am. Chem. Soc.* **1997**, *119*, 11236−11243. (e) Klei, S. R.; Tilley, T. D.; Bergman, R. G. *Organometallics* **2002**, *21*, 4648−4661. (f) Calimano, E.; Tilley, T. D. *Organometallics* **2010**, *29*, 1680−1692. (g) Fasulo, M.; Tilley, T. D. *Organometallics* **2012**, *31*, 5049−5057.
(7) (a) Gutsulyak, D. V.; Nikonov, G. I. *Angew. Chem., Int. Ed.* **2010**, *49*, 7553−7556. (b) Boone, C.; Korobkov, I.; Nikonov, G. I. *ACS Catal.* **2013**, *3*, 2336−2340. (c) Cheng, C.; Brookhart, M. *J. Am. Chem. Soc.* **2012**, *134*, 11304−11307. (d) Gutsulyak, D. V.; van der Est, A.; Nikonov, G. I. *Angew. Chem., Int. Ed.* **2011**, *50*, 1384−1387.
(8) Lipke, M. C.; Tilley, T. D. *J. Am. Chem. Soc.* **2011**, *133*, 16374−16377.
(9) Lipke, M. C.; Tilley, T. D. *J. Am. Chem. Soc.* **2013**, *135*, 10298−10301.
(10) For recent examples of ketone hydrosilation catalysts that exhibit high activity see reference 5b and (a) Yang, J.; Tilley, T. D. *Angew. Chem. Int., Ed.* **2010**, *49*, 10186−10188. (b) Gade, L. H.; César, V.; Bellemin-Lapponaz, S. *Angew. Chem., Int. Ed.* **2004**, *43*, 1014−1017. (c) Ruddy, a. J.; Kelly, C. M.; Crawford, S. M.; Wheaton, C. A.; Sydora, O. L.; Small, B. L.; Stradiotto, M.; Turculet, L. *Organometallics* **2013**, *32*, 5581−5588. (d) Chakraborty, S.; Blacque, O.; Fox, T.; Berke, H. *ACS Catal.* **2013**, *3*, 2208−2217.
(11) Lipke, M.c.; Neumeyer, F.; Tilley, T. D. *J. Am. Chem. Soc.* **2014**, *136*, 6092−6102.
(12) Zoellner, R. W. *J. Chem. Educ.* **1990**, *67*, 714−715. Note that errors provided for the molecular weight measurement on **4a** are based on those typical of this method, rather than derived from multiple repetitions of the experiment.
(13) (a) Nikonov, G. I. *Adv. Organomet. Chem.* **1995**, *53*, 217−309. (b) Lachaize, S.; Sabo-Etienne, S. *Eur. J. Inorg. Chem.* **2006**, 2115−2127.
(14) Liepinš, E.; Birğele, I.; Tomsons, P.; Lukevics, E. *Magn. Reson. Chem.* **1985**, *23*, 485−486.
(15) All DFT calculations were carried out with Gaussian 09 using the B3PW91 functional and 6-31G(d,p)/LANL 2DZ basis sets.
(16) Grumbine, S. K.; Straus, D. A.; Tilley, T. D. *Polyhedron* **1995**, *14*, 127−148.
(17) Delpech, F.; Sabo-Etienne, S.; Daran, J.-C.; Chaudret, B.; Hussein, K.; Marsden, C. J.; Barthelat, J.-C. *J. Am. Chem. Soc.* **1999**, *121*, 6668−6682.
(18) Chalk, A. J.; Harrod, J. F. *J. Am. Chem. Soc.* **1965**, *87*, 16−21.
(19) (a) Chakroborty, S.; Krause, J. A.; Guam, H. *Organometallics* **2009**, *28*, 582−586. (b) Peterson, E.; Khalimon, A. Y.; Simionescu, R.; Kuzmina, L. G.; Howard, J. A. K.; Nikonov, G. I. *J. Am. Chem. Soc.* **2009**, *131*, 908−909. (c) Issenhuth, J.-T.; Notter, F.-P.; Dagorne, S.; Dedieu, A.; Bellemin-Laponnaz, S. *Eur. J. Inorg. Chem.* **2010**, *4*, 529−541.
(20) (a) Du, G.; Fanwick, P. E.; Abu-Omar, M. M. *J. Am. Chem. Soc.* **2007**, *129*, 5180−5187. (b) Shirobokov, O. G.; Kuzmina, L. G.; Nikonov, G. I. *J. Am. Chem. Soc.* **2011**, *133*, 6487−6489.
(21) Corriu, R. J. P.; Guerin, C.; Henner, B.; Wang, Q. *Organometallics* **1991**, *10*, 2297−2303.
(22) Betley, T. A.; Peters, J. C. *Inorg. Chem.* **2003**, *42*, 5074−5084.
(23) Wiles, C.; Watts, P.; Haswell, S. J. *Tetrahedron Lett.* **2006**, *47*, 5261−5264.
(24) Wang, T.; Liang, Y.; Yu, Z.-X. *J. Am. Chem. Soc.* **2011**, *133*, 13762−13763.